The Astrophysical Journal, 981:101 (13pp), 2025 March 10 https://doi.org/10.3847/1538-4357/adb0bf

Estimating Black Hole Masses in Obscured Active Galactic Nuclei from X-Ray and Optical Emission Line Luminosities

Stephanie LaMassa[1], Isabella Farrow[2,3], C. Megan Urry[2,3], Benny Trakhtenbrot[4], Connor Auge[5], Michael J. Koss[5], Alessandro Peca[2,5], Dave Sanders[6], and Tracey Jane Turner[5]
[1] Space Telescope Science Institute, 3700 San Martin Drive, Baltimore, MD 21218, USA; slamassa@stsci.edu
[2] Department of Physics, Yale University, P.O. Box 201820, New Haven, CT 06520-8120, USA
[3] Yale Center for Astronomy and Astrophysics, P.O. Box 208121, New Haven, CT 06520, USA
[4] School of Physics and Astronomy, Tel Aviv University, Tel Aviv 69978, Israel
[5] Eureka Scientific, 2452 Delmer Street Suite 100, Oakland, CA 94602-3017, USA
[6] Institute for Astronomy, University of Hawaii, 2680 Woodlawn Drive, Honolulu, HI 96822, USA
Received 2023 December 8; revised 2025 January 8; accepted 2025 January 17; published 2025 March 3

Abstract

We test a novel method for estimating black hole masses ($M_{\rm BH}$) in obscured active galactic nuclei (AGN) that uses proxies to measure the FWHM of broad Hα (FWHM$_{\rm bH\alpha}$) and the accretion disk luminosity at 5100 Å ($\lambda L_{5100\ \text{Å}}$). Using a published correlation, we estimate FWHM$_{\rm bH\alpha}$ from the narrow optical emission line ratio $L_{[\rm O\ III]}/L_{\rm nH\beta}$. Using a sample of 99 local obscured AGN from the Swift Burst Alert Telescope AGN Spectroscopic Survey (BASS), we assess the agreement between estimating $\lambda L_{5100\ \text{Å}}$ from the intrinsic 2 to 10 keV X-ray luminosity and from narrow optical emission lines. We find a mean offset of 0.32 ± 0.68 dex between these methods, which propagates to a factor of ∼2 uncertainty when estimating $M_{\rm BH}$ using a virial mass formula where $L_{[\rm O\ III]}/L_{\rm nH\beta}$ serves as a proxy of FWHM$_{\rm bH\alpha}$ ($M_{\rm BH,[O\ III]/nH\beta}$). We compare $M_{\rm BH,[O\ III]/nH\beta}$ with virial $M_{\rm BH}$ measurements from broad Paschen emission lines. For the 14 (12) BASS AGN with broad Paα (Paβ) detections, we find $M_{\rm BH,[O\ III]/nH\beta}$ to be systematically higher than $M_{\rm BH,Pa\alpha}$ ($M_{\rm BH,Pa\beta}$) by a factor of 0.39 ± 0.44 dex (0.48 ± 0.51 dex). Since these offsets are within the scatter, more data are needed to assess whether $M_{\rm BH,[O\ III]/nH\beta}$ is biased high. For 151 BASS AGN with measured stellar velocity dispersions (σ_*), we find that the σ_*-derived $M_{\rm BH}$ agrees with $M_{\rm BH,[O\ III]/nH\beta}$ to within 0.08 dex, albeit with wide scatter (0.74 dex). The method tested here can provide estimates of $M_{\rm BH}$ in thousands of obscured AGN in spectroscopic surveys when other diagnostics are not available, though with an uncertainty of ∼3–5.

Unified Astronomy Thesaurus concepts: Supermassive black holes (1663); X-ray astronomy (1810); Seyfert galaxies (1447); Active galactic nuclei (16)

Materials only available in the online version of record: machine-readable tables

1. Introduction

The mass of a black hole ($M_{\rm BH}$) is one if its fundamental properties (C. W. Misner et al. 1973). A primary mechanism of black hole growth is via accretion of nearby matter. Steady accretion onto supermassive black holes (SMBHs; $M_{\rm BH} \geqslant 10^6\ M_\odot$) in the centers of galaxies produce active galactic nuclei (AGN), which are the most luminous, persistent objects in the Universe (D. E. Osterbrock 1993). Studying AGN thus provides us a way to constrain the growth history of massive black holes over cosmic time, as long as the mass of the black hole can be measured.

In nearby nonactive galaxies where the central region of the galaxy can be resolved, the SMBH mass can be estimated by measuring the kinematics of the stars and/or gas moving around the black hole. Indeed, decades of mapping out the motions of stars in the center of our own Milky Way galaxy provided the strongest evidence yet of a quiescent black hole, Sagittarius A*, of mass $4 \times 10^6\ M_\odot$ (A. M. Ghez et al. 1998, 2008; R. Genzel et al. 2000, 2010). Applying kinematic analysis to neighboring galaxies provides dynamical measurements of SMBH masses, along with the discovery of a correlation between properties of the host galaxy (velocity stellar dispersion, bulge luminosity, and total stellar mass) and the SMBH mass (J. Kormendy & D. Richstone 1995; J. Magorrian et al. 1998; L. Ferrarese & D. Merritt 2000; L. Ferrarese et al. 2001; K. Gebhardt et al. 2000; K. Gültekin et al. 2009; J. Kormendy & L. C. Ho 2013; A. E. Reines & M. Volonteri 2015).

These methods are inapplicable to unobscured AGN as emission from the accretion disk dominates over that of the host galaxy, precluding the ability to resolve and measure the motion of stars or gas within the sphere of influence of the black hole. The motion of gas near the black hole ionized by the accretion disk can be used to derive the $M_{\rm BH}$ as long as the distance to these gas clouds can be measured. From reverberation mapping, we can measure how the broad emission line profiles from ionized gas in the broad-line region (BLR) respond to accretion-driven luminosity fluctuations (see B. M. Peterson 2014, for a review). These reverberation mapping campaigns are necessarily time intensive, spanning months to years, and though have accurately measured AGN black hole masses for hundreds of AGN (e.g., Y. Shen et al. 2015, 2019, 2024; C. J. Grier et al. 2017, 2019; Y. Homayouni et al. 2020), this method does not easily scale to tens of thousands of AGN.

But these campaigns have been critical for establishing that the accretion disk luminosity serves as a proxy of the distance

to the black hole (e.g., M. C. Bentz et al. 2006, 2009; S. Kaspi et al. 2005). The gas orbital speed can be estimated by the width of emission lines in the BLR, allowing the black hole mass to be measured from single-epoch spectra ($M_{\rm BH} = f\frac{Rv^2}{G}$; where R is the distance between black hole and ionized gas, v is the gas orbital speed, f is the scale factor that depends on the kinematics and geometry of the BLR, and G is the gravitational constant). Different single-epoch spectra virial mass relationships have been calibrated for emission lines from the ultraviolet (C IV 1549 Å and Mg II 2800 Å; M. Vestergaard & B. M. Peterson 2006; Y. Shen et al. 2011; B. Trakhtenbrot & H. Netzer 2012), through the optical (Hβ 4861 Å and Hα 6563 Å; M. Vestergaard & B. M. Peterson 2006; J. E. Greene et al. 2010), to the near-infrared (NIR; Paβ 12822 Å and Paα 18751 Å; D. Kim et al. 2010). Each mass scaling relationship has an uncertainty of 0.18–0.6 dex, and the agreement between $M_{\rm BH}$ values calibrated from different emission lines can vary by a factor of 0.12–0.4 dex (Y. Shen & X. Liu 2012; B. Trakhtenbrot & H. Netzer 2012).

These methods of estimating black hole masses only work when we have a direct view of the accretion disk and BLR. Most AGN are obscured (C. Ramos Almeida & C. Ricci 2017; R. C. Hickox & D. M. Alexander 2018) such that this central region is blocked by large amounts of dust and gas. One of the best ways to measure SMBH masses in obscured AGN is to measure accretion disk Keplerian velocities from water maser emission at $\lambda = 1.35$ cm (J. M. Moran et al. 1999), but only a small percentage of AGN are in favorable conditions and nearby for water maser emission to be detected (G. Zhu et al. 2011). A common way to estimate black hole masses in obscured AGN is to leverage the correlation between the dynamical mass of SMBHs and velocity dispersion of stars in the galaxy (σ_*), which has an intrinsic scatter of ∼0.3 dex (see J. Kormendy & L. C. Ho 2013, for a review), though the spread can be as high as ∼0.5 dex (C. Marsden et al. 2020), and there is evidence that M_BH values calculated from sigma_star may be overestimated in obscured AGN (J. E. Greene et al. 2016, F. Ricci et al. 2017c, M. Gliozzi et al. 2024). Accurate measurements of the stellar velocity dispersion requires high-quality spectra, which are prohibitively difficult to obtain for large samples of AGN beyond the very local Universe ($z > 0.1$; M. J. Koss et al. 2022c).

A promising technique to estimate black hole masses in obscured AGN was presented by D. Baron & B. Ménard (2019, hereafter BM19). Using a sample of 1941 unobscured (Type 1) AGN at $z < 0.3$ from Data Release 7 of the Sloan Digital Sky Survey (SDSS; D. G. York et al. 2000; K. N. Abazajian et al. 2009), they found that the AGN ionization field hardness (traced by the ratio of the narrow [O III] λ5007 to narrow Hβ (nHβ) line, $L_{\rm [O\,III]}/L_{\rm nH\beta}$) in the narrow-line region (NLR) correlates with BLR kinematics (parameterized by the FWHM of broad Hα (FWHM$_{\rm bH\alpha}$)), though it is unclear what physically links the BLR kinematics to the NLR ionization to give rise to this correlation. Since the key ingredients for measuring $M_{\rm BH}$ in virial mass formulas are the BLR kinematics and accretion disk luminosity, this empirical correlation found by BM19 implies that $L_{\rm [O\,III]}/L_{\rm nH\beta}$ can be used as a proxy of FWHM$_{\rm bH\alpha}$ to calculate $M_{\rm BH}$ (hereafter $M_{\rm BH,[O\,III]/nH\beta}$). The other key parameter in virial black hole mass formulas, the accretion disk luminosity, is invisible in obscured AGN. BM19 suggest that the accretion disk luminosity at 5100 Å ($\lambda L_{5100\ \text{Å}}$) can be estimated from either narrow optical emission lines (H. Netzer 2009) or the intrinsic 2–10 keV luminosity (R. Maiolino et al. 2007) in order to calculate $M_{\rm BH,[O\,III]/nH\beta}$.

BM19 applied their technique to calculate black hole masses for 10,000 obscured (Type 2) AGN from SDSS where they estimated $\lambda L_{5100\ \text{Å}}$ from narrow optical emission lines and FWHM$_{\rm bH\alpha}$ from $L_{\rm [O\,III]}/L_{\rm nH\beta}$. When comparing these black hole masses with the host galaxy stellar velocity dispersion, they found a scatter of ∼0.45 dex, comparable to quoted uncertainties in $M_{\rm BH}$–σ_* relations (J. Kormendy & L. C. Ho 2013; C. Marsden et al. 2020), leading them to conclude that $M_{\rm BH,[O\,III]/nH\beta}$ is a reliable way to estimate black hole mass. Some studies have since used the BM19 method to calculate $M_{\rm BH,[O\,III]/nH\beta}$ for Type 2 AGN (A. Ferré-Mateu et al. 2021; S.-C. Rey et al. 2021; G. Vietri et al. 2022; M. Siudek et al. 2023) and a larger number of studies have compared theoretical predictions of $M_{\rm BH}$/host galaxy correlations with the BM19 $M_{\rm BH,[O\,III]/nH\beta}$ sample (F. Shankar et al. 2020; M. Volonteri et al. 2020; Y. Dubois et al. 2021; M. Habouzit et al. 2021; M. Trebitsch et al. 2021; A. Trinca et al. 2022; R. S. Beckmann et al. 2023; F. Sassano et al. 2023). Though the BM19 formulation to estimate $M_{\rm BH}$ is being adopted, this technique has only been tested on indirect methods of measuring $M_{\rm BH}$ (i.e., correlating $M_{\rm BH}$ with σ_*). BM19 caution that their technique cannot be reliably tested on Type 1 AGN due to the uncertainty in decomposing the nHβ emission line from the broad component. They instead point out that a direct test would be to identify a sample of AGN with no broad Hβ emission but with broad Paα or Paβ lines detected from which the virial black hole mass can be calculated (D. Kim et al. 2010; H. Landt et al. 2011a, 2011b, 2013). Since the Paschen series lie in the NIR, these lines are less affected by dust obscuration that extinguishes the optical emission, so it is possible for some AGN to show both narrow Balmer lines and broad Paschen lines.

We perform this test using local ($z \leqslant 0.3$) obscured AGN detected from the ultrahard X-ray (14–195 keV) Neil Gehrels Swift Observatory (Swift) Burst Alert Telescope (BAT) sample, which has extensive optical and infrared spectroscopic data available from the BAT AGN Spectroscopic Survey (BASS; M. Koss et al. 2017; I. Lamperti et al. 2017; F. Ricci et al. 2017b; J. S. den Brok et al. 2022; M. J. Koss et al. 2022b; K. Oh et al. 2022). Using this data set, we compare estimates of $\lambda L_{5100\ \text{Å}}$ derived from the intrinsic X-ray luminosity between 2 and 10 keV ($L_{\rm 2-10\ keV}$; R. Maiolino et al. 2007; E. Lusso et al. 2010) and from the optical emission line luminosities (H. Netzer 2009). We note that the empirical relationships we are testing to estimate FWHM$_{\rm bH\alpha}$ and $\lambda L_{5100\ \text{Å}}$ were calibrated on Type 1 AGN and we are applying these relationships to obscured AGN, which may not be appropriate if there are systematic differences in these quantities between unobscured and obscured AGN. However, our intention is to investigate how well these empirical relationships perform when estimating $M_{\rm BH}$ in obscured AGN; any systematic differences will contribute to the observed spread and quoted uncertainty in black hole mass measurements. We test whether a correlation exists between $L_{\rm [O\,III]}/L_{\rm nH\beta}$ and the BLR kinematics traced by the Paα and Paβ FWHM values. We then calculate the black hole masses for AGN using the single-epoch spectrum virial mass equations for Paα and Paβ and compare those with $M_{\rm BH,[O\,III]/nH\beta}$. Finally, for a larger sample of BASS AGN, we compare $M_{\rm BH,[O\,III]/nH\beta}$ with black hole masses derived from

Table 1
Number of Active Galactic Nuclei in Each Subsample

Sample	$M_{\rm BH,[O\ III]/nH\beta}$	$\lambda L_{5100\ \text{Å}}$	Broad Paα	Broad Paβ	σ_*
$M_{\rm BH,[O\ III]/nH\beta}$[a]	172	99	14	12	151
$\lambda L_{5100\ \text{Å}}$[b]	99	99	2	2	94
Broad Paα[c]	14	2	14	8	12
Broad Paβ[d]	12	2	8	12	10
σ_*[e]	151	94	12	10	151

Notes.
[a] Parent sample of BASS AGN with [O III] detected, nHβ detected, intrinsic 2–10 keV flux measured, no broad Hβ component detected, and within the ionization hardness range of 0.55 dex $<\log(L_{\rm [O\ III]}/L_{\rm nH\beta})<$ 1.05.
[b] Subset of parent sample with narrow Hα (nHα) detected and no broad Hα component detected, used to compare proxies for estimating $\lambda L_{5100\ \text{Å}}$.
[c] Subset of parent sample with broad Paα detected.
[d] Subset of parent sample with broad Paβ detected.
[e] Subset of parent sample with measured stellar velocity dispersions.

σ_*. For reference, we use a flat cosmology where $H_0 = 67.7$ km s^{-1} Mpc^{-1} and $\Omega_m = 0.307$ (Planck Collaboration et al. 2016).

2. Sample Selection

We select AGN from the BASS sample (M. Koss et al. 2017; M. J. Koss et al. 2022b) for this analysis due to the homogeneity, multiwavelength completeness, and quality of this data set. The BAT (S. D. Barthelmy et al. 2005) on board Swift (N. Gehrels et al. 2004) is sensitive to ultrahard X-rays (14−195 keV) and has detected hundreds of AGN. The BASS survey provides extensive multiwavelength follow-up of these ultrahard X-ray-selected AGN, ranging from NIR (I. Lamperti et al. 2017; F. Ricci et al. 2017b; J. S. den Brok et al. 2022) and optical (e.g., M. J. Koss et al. 2022c; K. Oh et al. 2022) spectroscopy to detailed X-ray analysis using softer X-ray data (0.5–10 keV) from Chandra, XMM-Newton, and Swift's X-Ray Telescope (C. Ricci et al. 2017a).

To begin, we identify BASS AGN that have [O III] λ5007, nHβ, and intrinsic 2–10 keV X-ray fluxes measured, as well as no broad component to Hβ detected (F. Ricci et al. 2017b; K. Oh et al. 2022). Details about fitting the optical emission lines are provided in K. Oh et al. (2022), but in short the spectra were initially fitted with narrow emission lines and when the spectra were not well described by these fits, broad Gaussian components with an FWHM above 1000 km s^{-1} were added. K. Oh et al. (2022) report fluxes for emission lines if the Gaussian amplitude over noise ratio exceeded three.[7] They provide a flag in their published tables to indicate whether a broad Balmer line is used in the spectral fit. We filtered their table to identify the AGN where they flagged that no broad component was used to fit Hβ.

BM19 demonstrate that the correlation they found between $L_{\rm [O\ III]}/L_{\rm nH\beta}$ and FWHM$_{\rm bH\alpha}$ holds for $\log(L_{\rm [O\ III]}/L_{\rm nH\beta}) >$ 0.55 dex, which is the cutoff at which AGN ionization dominates over star formation in powering the [O III] line flux (J. A. Baldwin et al. 1981; L. J. Kewley et al. 2001). Their sample has an upper limit of $\log(L_{\rm [O\ III]}/L_{\rm nH\beta}) < 1.05$ dex. We apply both cuts on the ionization hardness to the BASS data set, giving us a parent sample of 172 AGN (Table 1).

For our first test, we compare the agreement between two methods of estimating the accretion disk luminosity at 5100 Å (i.e., $\lambda L_{5100\ \text{Å}}$). In obscured AGN, the accretion disk is blocked from view and $\lambda L_{5100\ \text{Å}}$ can therefore not be directly measured. However, there are methods to estimate $\lambda L_{5100\ \text{Å}}$ based on the intrinsic X-ray luminosity (S. Kaspi et al. 2005; R. Maiolino et al. 2007; E. Lusso et al. 2010) and optical narrow emission line fluxes (H. Netzer 2009). This latter method requires a reddening correction calculated from the ratio of the nHα and nHβ lines. We therefore identify a subsample where nHα is detected without a broad Hα component. This selection provides 99 AGN for quantifying the consistency between $\lambda L_{5100\ \text{Å}}$ proxies.

We assess the consistency between black hole masses calculated using the BM19 method with measurements of the virial mass calculated from broad Paα and Paβ emission lines. Using data from I. Lamperti et al. (2017), F. Ricci et al. (2022), and J. S. den Brok et al. (2022), we identify AGN where the quality of the fit to the Paschen lines was deemed very good (FLAG == 1) or acceptable (FLAG == 2).[8] Of the 172 AGN in the BASS parent sample, we find 14 and 12 AGN with broad Paα and broad Paβ detected, respectively; eight AGN have both broad Paα and broad Paβ detected. Finally, we use the measured stellar velocity dispersions of 151 BASS AGN (M. J. Koss et al. 2022c) to indirectly estimate $M_{\rm BH}$ from the $M_{\rm BH}-\sigma_*$ relation, and compare those estimates with $M_{\rm BH}$ measured from the BM19 method.

The optical spectra were collected from telescopes with aperture slit widths between 1″ and 3″ (M. J. Koss et al. 2022a). The projected size of the optical spectroscopic apertures cover >600 pc of the AGN host galaxy for over 78% of the BASS AGN. This scale is consistent with the physical scales probed by the SDSS aperture in the BM19 AGN sample (0.6–12 kpc), making the BASS sample an appropriate one to test the efficacy of a relationship calibrated on SDSS AGN. We note that the infrared spectroscopic apertures cover smaller scales (projected sizes of 0.09–1.6 kpc; I. Lamperti et al. 2017; J. S. den Brok et al. 2022; F. Ricci et al. 2022), but here we are probing emission from the compact BLR where smaller apertures are appropriate to minimize host galaxy dilution.

[7] Amplitude over noise ratios are a typical metric used to claim an emission line as significant. The amplitude is the height of the Gaussian function and noise is determined from the rms between the data and the model in the continuum on either side of the emission line.

[8] Only the catalogs of I. Lamperti et al. (2017) and F. Ricci et al. (2022) provide this spectral fitting information. We include all Paα or Paβ measurements from the J. S. den Brok et al. (2022) catalog under the assumption that all of these published values are reliable.

Table 2
BASS Analysis Sample[a]

ID	Swift-BAT Name	R.A. (deg)	Decl. (deg)	z	$\lambda L_{5100\ \text{Å}}$ Sample	Paα Sample	Paβ Sample	σ_* Sample
63	SWIFTJ0114.4-5522	18.6039	−55.397	0.0124	N	N	Y	Y
72	SWIFTJ0123.8-3504	20.9765	−35.065	0.019	N	Y	Y	Y
226	SWIFTJ0433.0+0521	68.2962	5.354	0.0334	N	Y	Y	N
404	SWIFTJ0804.2+0507	121.024	5.114	0.013	Y	Y	N	Y
511	SWIFTJ1042.4+0046	160.535	0.702	0.095	N	Y	Y	Y
586	SWIFTJ1204.5+2019	181.124	20.316	0.0229	N	Y	N	Y
682	SWIFTJ1338.2+0433	204.566	4.543	0.023	N	N	Y	Y
698	SWIFTJ1353.7-1122	208.368	−11.385	0.0687	N	Y	N	Y
700	SWIFTJ1354.5+1326	208.621	13.466	0.063	Y	Y	N	Y
738	SWIFTJ1441.4+5341	220.159	53.504	0.0377	N	Y	N	Y
757	SWIFTJ1508.8-0013	227.225	−0.197	0.0545	N	Y	Y	Y
971	SWIFTJ1824.2+1845	276.045	18.769	0.0663	N	Y	N	Y
1027	SWIFTJ1913.3-5010	288.311	−50.183	0.062	Y	N	Y	Y
1060	SWIFTJ2001.0-1811	300.232	−18.174	0.037	N	Y	Y	Y
1090	SWIFTJ2044.2-1045	311.041	−10.724	0.0347	N	Y	Y	N
1138	SWIFTJ2204.7+0337	331.08	3.564	0.0611	Y	N	Y	Y
1157	SWIFTJ2235.9-2602	338.943	−26.05	0.0049	N	Y	Y	Y
1161	SWIFTJ2236.7-1233	339.194	−12.545	0.024	N	Y	Y	Y

Note.
[a] The BASS AGN sample is presented in M. Koss et al. (2017) and M. J. Koss et al. (2022b). We use optical emission line fluxes from K. Oh et al. (2022), NIR emission line fluxes from I. Lamperti et al. (2017), F. Ricci et al. (2022), and J. S. den Brok et al. (2022), and X-ray fluxes from C. Ricci et al. (2017a). We show here a subset of this table for illustrative purposes. The catalog is available in its entirety online.

(This table is available in its entirety in machine-readable form in the online article.)

Table 3
BASS Active Galactic Nucleus Fluxes and Paschen FWHM Values[a]

ID	$F_{\text{nH}\beta}$ (10^{-14} erg s^{-1})	$F_{[\text{O III}]}$ (10^{-14} erg s^{-1})	$F_{\text{H}\alpha}$ (10^{-14} erg s^{-1})	$F_{\text{Pa}\alpha}$ (10^{-14} erg s^{-1})	FWHM$_{\text{Pa}\alpha}$ (km s^{-1})	$F_{\text{Pa}\beta}$ (10^{-14} erg s^{-1})	FWHM$_{\text{Pa}\beta}$ (km s^{-1})	$F_{2-10\ \text{keV, intrinsic}}$ (10^{-14} erg s^{-1})
63	0.53	2.66	⋯	⋯	⋯	1.58	1430	4.50
72	0.78	8.41	⋯	17.4	5220	6.59	6670	22.4
226	9.47	49.0	⋯	33.6	2606	23.9	2842	38.2
404	8.02	64.4	29.0	1.90	3156	⋯	⋯	32.9
511	0.28	1.60	⋯	1.53	2520	0.50	1320	3.10
586	1.35	11.5	⋯	2.39	3970	⋯	⋯	7.00
682	1.60	8.56	⋯	⋯	⋯	2.89	6189	10.8
698	0.15	1.16	⋯	1.19	6449	⋯	⋯	6.00
700	0.41	4.23	1.36	0.53	6159	⋯	⋯	4.10
738	9.39	50.9	⋯	2.30	2173	⋯	⋯	5.50
757	1.41	14.5	⋯	4.10	6783	9.09	8229	8.10
971	0.99	8.47	⋯	5.49	9446	⋯	⋯	4.10
1027	0.06	0.28	0.32	⋯	⋯	0.88	2720	8.40
1060	0.21	1.32	⋯	17.7	4412	7.70	4362	6.30
1090	8.14	37.0	⋯	61.4	3133	43.8	2918	44.1
1138	2.16	17.4	8.64	⋯	⋯	0.84	3220	7.20
1157	0.56	4.30	⋯	4.30	1570	2.84	1420	41.8
1161	6.15	46.4	⋯	5.53	2571	4.43	4325	11.7

Notes.
[a] The optical emission line measurements are from K. Oh et al. (2022), the NIR line measurements are from I. Lamperti et al. (2017), F. Ricci et al. (2022), and J. S. den Brok et al. (2022), and the X-ray fluxes are from C. Ricci et al. (2017a). We show here a subset of this table for illustrative purposes. The catalog is available in its entirety online.
[b] The [O III] fluxes reported in K. Oh et al. (2022) have a reddening correction applied. In our analysis, we back out this correction using their reported correction factor so that we are using the observed [O III] flux.

(This table is available in its entirety in machine-readable form in the online article.)

In Table 2, we identify the BASS AGN used for this analysis and the sample(s) in which they belong. We list the emission line fluxes, intrinsic 2–10 keV X-ray fluxes, and infrared fluxes and FWHM values in Table 3.

3. Analysis

To calculate the black hole masses of obscured AGN, we use Equation (5) from BM19, which was derived using the radius–luminosity relation reported in M. C. Bentz et al. (2013) and

the correlation between $\mathrm{FWHM_{bH\alpha}}$ and $\mathrm{FWHM_{bH\beta}}$ derived in J. E. Greene & L. C. Ho (2005):

$$\log\left(\frac{M_{\rm BH}}{M_\odot}\right) = \log\epsilon + 6.90 + 0.54 \times \log\left(\frac{\lambda L_{5100\,\text{Å}}}{10^{44}\ \mathrm{erg\ s^{-1}}}\right) + 2.06 \times \log\left(\frac{\mathrm{FWHM_{bH\alpha}}}{10^{3}\ \mathrm{km\ s^{-1}}}\right). \quad (1)$$

Here, we assume the scaling factor (ϵ) in their Equation (5) is unity. While it is challenging to determine the geometric scale factor for individual AGN due to unknowns in the BLR geometry, inclination, and kinematics, the average value for this virial factor is approximately unity when using the FWHM of broad emission lines to calculate $M_{\rm BH}$ (e.g., see J.-H. Woo et al. 2015). Published papers from the BASS survey adopt a geometric scaling factor of unity when calculating $M_{\rm BH}$ where the virial motion of the gas is measured from the FWHM of the broad line (note that $\epsilon = 1$ corresponds to a virial factor of 5.5 when using the line velocity dispersion as a proxy of gas orbital speed; J. S. den Brok et al. 2022; J. E. Mejía-Restrepo et al. 2022) and we adopt this convention in the current analysis for consistency, especially when comparing our $M_{\rm BH,[O\,III]/nH\beta}$ values with those derived from NIR Paschen virial mass equations. We note that this scale factor is calculated for Type 1 AGN where the inclination of the BLR is putatively aligned face on and we are assuming this factor is a reasonable starting point to estimate $M_{\rm BH}$ in edge-on AGN: such uncertainties in the geometric scale factor will contribute to uncertainties in the final $M_{\rm BH,[O\,III]/nH\beta}$ values.

To solve Equation (1), we need both an estimate of the accretion disk luminosity $\lambda L_{5100\,\text{Å}}$ and the FWHM of the broad Hα line. $\mathrm{FWHM_{bH\alpha}}$ can be derived from the $L_{\rm [O\,III]}/L_{\rm nH\beta}$ ratio using Equation (1) from BM19, which we recast as:

$$\log\left(\frac{\mathrm{FWHM_{bH\alpha}}}{10^{3}\ \mathrm{km\ s^{-1}}}\right) = (1.72 \pm 0.21) \times \log\left(\frac{L_{\rm [O\,III]}}{L_{\rm nH\beta}}\right) - (0.62 \pm 0.19). \quad (2)$$

3.1. Estimating Accretion Disk Luminosity at 5100 Å: $\lambda L_{5100\,\text{Å}}$

The ultraviolet to optical emitting accretion disk is hidden in obscured AGN meaning that $\lambda L_{5100\,\text{Å}}$ cannot be measured directly from the optical spectrum. There are proxies for estimating $\lambda L_{5100\,\text{Å}}$ that are derived by relations observed in unobscured AGN. One proxy comes from the optical narrow emission lines (herein dubbed $\lambda L_{5100\,\text{Å,nel}}$) and another comes from the intrinsic 2–10 keV luminosity (hereafter $\lambda L_{5100\,\text{Å,X-ray}}$). Both methods have advantages and drawbacks in their applicability to AGN detected in surveys.

The optical method requires a reddening correction to the narrow line to be calculated via the Balmer decrement (nHα/nHβ). This method is applicable to thousands of AGN from ground-based optical surveys at $z < 0.5$ (beyond which Hα is redshifted into the infrared) and can be used for infrared spectroscopic studies of higher redshift AGN up to $z < 1$, after which the $L_{\rm [O\,III]}/L_{\rm nH\beta}$ ratio for star-forming galaxies increases (L. J. Kewley et al. 2013).

The X-ray method can be a powerful technique to use for tens of thousands of AGN detected in X-ray surveys and can in principle be used at any redshift. However, this method requires that the intrinsic X-ray luminosity be known via high-fidelity spectral modeling, which is hard to accurately measure for AGN with low X-ray flux, including highly obscured AGN and those at high redshift, due to a combination of generally low spectral quality and the number of model parameters needed to constrain the obscuring column density. Due to the proximity of the BASS AGN and the significant time investment in observing these sources with X-ray facilities, the spectra of many of these AGN were of high quality to permit sophisticated spectral modeling (see C. Ricci et al. 2017a, for details).

Here, we test the agreement between these two methods of estimating $\lambda L_{5100\,\text{Å}}$ in obscured AGN.

3.1.1. $\lambda L_{5100\,\text{Å,nel}}$: Estimating $\lambda L_{5100\,\text{Å}}$ from Optical Narrow Emission Lines

First we derive a formula for $\lambda L_{5100\,\text{Å,nel}}$ using previously published relationships that link the 5100 Å luminosity to the bolometric luminosity, and the bolometric luminosity to optical narrow emission lines. Using the relationship found between $\lambda L_{5100\,\text{Å}}$ and the isotropic AGN luminosity ($L_{\rm iso}$), we have from J. C. Runnoe et al. (2012):

$$\log\left(\frac{\lambda L_{5100,\rm optical}}{10^{44}\ \mathrm{erg\ s^{-1}}}\right) = 1.0965 \times \log\left(\frac{L_{\rm bol}}{10^{44}\ \mathrm{erg\ s^{-1}}}\right) - 0.98. \quad (3)$$

This formula assumes $L_{\rm bol} \approx 0.75\ L_{\rm iso}$ to correct for anisotropy in the viewing angle of the accretion disk (see J. C. Runnoe et al. 2012).

H. Netzer (2009) demonstrated that $L_{\rm bol}$ can be estimated using the luminosity of the reddening-corrected nHβ line ($L_{\rm nH\beta,corr}$) and the ratio of the observed [O III] luminosity to observed nHβ luminosity:

$$\log\left(\frac{L_{\rm bol}}{10^{44}\ \mathrm{erg\ s^{-1}}}\right) = \log\left(\frac{L_{\rm nH\beta,corr}}{10^{40}\ \mathrm{erg\ s^{-1}}}\right) - 0.25 + \max\left[0,\ 0.31\left(\log\frac{L_{\rm [O\,III]}}{L_{\rm nH\beta}} - 0.6\right)\right]. \quad (4)$$

We emphasize that this equation assumes a Galactic reddening relation (J. A. Cardelli et al. 1989) rather than the $\lambda^{-0.7}$ extinction law from S. Charlot & S. M. Fall (2000) that was considered in H. Netzer (2009). We note that the equation in BM19 uses the $\lambda^{-0.7}$ extinction law, but then a Galactic extinction curve to derive the reddening correction to the nHβ line. Here, we assume the Galactic extinction law throughout for internal consistency and for consistency with previous optical analysis of obscured AGN (e.g., L. Bassani et al. 1999; S. M. LaMassa et al. 2009, 2010; K. Oh et al. 2022).

Assuming Case B recombination in the AGN NLR (D. E. Osterbrock & G. J. Ferland 2006) and the extinction curve of J. A. Cardelli et al. (1989), we calculate the reddening-corrected nHβ luminosity as:

$$L_{\rm nH\beta,corr} = \left(\frac{L_{\rm nH\alpha}/L_{\rm nH\beta}}{3.1}\right)^{3.37} \times L_{\rm nH\beta}, \quad (5)$$

(see Appendix D of S. M. LaMassa et al. 2023, for a derivation). This correction is only applied if the observed ratio between nHα and nHβ exceeds 3.1.

If we were to use the $\lambda^{-0.7}$ extinction law instead, this would change both the normalization in Equation (4) (from −0.25 to −0.52) and the form of the reddening correction to $L_{\mathrm{nH}\beta,\mathrm{corr}} = \left(\frac{L_{\mathrm{nH}\alpha}\,/\,L_{\mathrm{nH}\beta}}{3.1}\right)^{5.28} \times L_{\mathrm{nH}\beta}$. For the BASS AGN, the J. A. Cardelli et al. (1989) extinction law produces an L_{bol} value that ranges from 0.14 to 1.86 times the L_{bol} value found using the $\lambda^{-0.7}$ extinction law, with a median difference of 1.28. Propagating these differences into Equations (3) and (1), the choice of the optical attenuation law can affect the derived black hole mass by a factor of 0.31–1.45, with a median difference of 1.16.

3.1.2. $\lambda L_{5100\ \text{Å,X-ray}}$: Estimating $\lambda L_{5100\ \text{Å}}$ from the Intrinsic X-Ray Luminosity

There is a connection between the ultraviolet emission (2500 Å) from the accretion disk and soft X-ray emission (2 keV) from the corona. This relationship is parameterized by α_{OX}, which is the slope of a power-law spectrum that connects the optical to X-ray emission (H. Tananbaum et al. 1979). This relationship can be used to estimate the optical continuum luminosity from the intrinsic X-ray luminosity (see, e.g., R. Maiolino et al. 2007). Using a sample of X-ray-selected Type 1 AGN from the XMM-COSMOS survey (G. Hasinger et al. 2007; N. Cappelluti et al. 2009), E. Lusso et al. (2010) quantified a relationship between the monochromatic X-ray luminosity at 2 keV and ultraviolet continuum luminosity at 2500 Å. Starting from this relationship, we derive an equation that links the intrinsic integrated 2–10 keV luminosity to the 5100 Å continuum luminosity (see the Appendix for the derivation):

$$\log\left(\frac{\lambda L_{5100\text{Å,X}-\mathrm{ray}}}{10^{44}\ \mathrm{erg\ s^{-1}}}\right) = 1.316 \times \log\left(\frac{L_{2-10\ \mathrm{keV,intrinsic}}}{10^{43}\ \mathrm{erg\ s^{-1}}}\right) - 1.378. \quad (6)$$

3.1.3. Comparing Proxies of $\lambda L_{5100\ \text{Å}}$

In Figure 1, we compare $\lambda L_{5100\ \text{Å,nel}}$ with $\lambda L_{5100\ \text{Å,X-ray}}$ for the 99 AGN for which there is only an nHα component detected and we can thus use the Balmer decrement to calculate $L_{\mathrm{nH}\beta,\mathrm{corr}}$ and then estimate $\lambda L_{5100\ \text{Å,nel}}$. As summarized in Table 4, we find a mean offset (i.e., $\log(\lambda L_{5100\ \text{Å,X-ray}}) - \log(\lambda L_{5100\ \text{Å,optical}})$ of −0.32 dex with a large scatter of 0.68 dex. Though there is an average offset, the wide scatter indicates that the quantities are statistically equal, though the scatter of up to a factor of 5 propagates into black hole mass uncertainties up to a factor of 2 (see Equation (1)). For completeness, we quantify the relationship between $\lambda L_{5100\ \text{Å,nel}}$ and $\lambda L_{5100\ \text{Å,X-ray}}$ by using a linear least squares fitter (LINEARLSQFITTER in astropy). Though we find a linear relationship above the one-to-one line, the 95% prediction interval to the linear fit overlaps the one-to-one relation due to the wide scatter in the fit residuals ($\sigma_{\mathrm{residual}}$).

Since we have intrinsic X-ray luminosity measurements for a larger number of AGN than those that have only nHα emission detected, we use $\lambda L_{5100\ \text{Å,X-ray}}$ as $\lambda L_{5100\ \text{Å}}$, together with Equation (2), as input into Equation (1). From this formula, we calculate the $L_{[\mathrm{O\ III}]}/L_{\mathrm{nH}\beta}$-derived black hole masses ($M_{\mathrm{BH,[O\ III]}/\mathrm{nH}\beta}$) and report these values in Table 5.

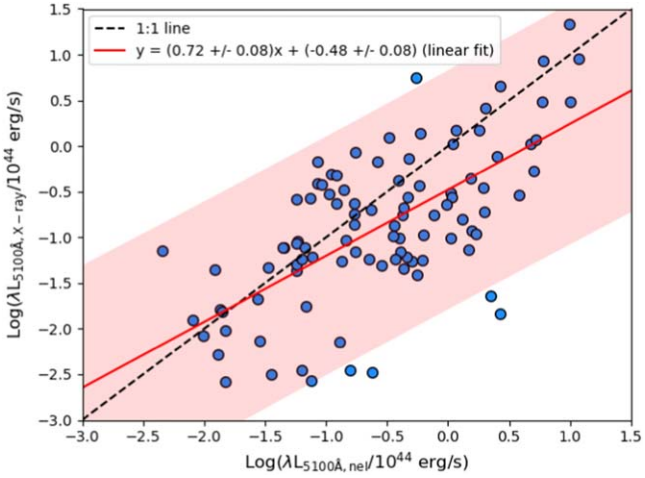

Figure 1. Comparison of estimates of the accretion disk luminosity at 5100 Å ($\lambda L_{5100\ \text{Å}}$) using optical narrow emission lines ($\lambda L_{5100\ \text{Å,nel}}$) and the intrinsic 2–10 keV luminosity ($\lambda L_{5100\ \text{Å,X-ray}}$) as a proxy. The black dashed line indicates the one-to-one relation, the red solid line is a linear fit to the data, and the shaded red region shows the 95% prediction interval for the linear fit. The mean offset (i.e., $\log(L_{5100\ \text{Å,X-ray}}) - \log(L_{5100\ \text{Å,nel}})$) is −0.32 ± 0.68 dex. While these quantities are statistically equal, this scatter of ∼5 in $\lambda L_{5100\ \text{Å}}$ can propagate to uncertainties of ∼2 in black hole mass estimates when using Equation (1). Error bars are not shown here since they are generally smaller than the size of the symbols.

3.2. Correlation between Narrow-line Region Ionization Hardness and Near-infrared Broad-line Region Kinematics?

The utility of $\log(L_{[\mathrm{O\ III}]}/L_{\mathrm{nH}\beta})$ as a parameter to estimate black hole mass relies on its observed correlation with the FWHM of Hα, which traces the virial motion of gas in the BLR. D. Kim et al. (2010) demonstrated that the FWHMs of the NIR Paschen lines Paα and Paβ are well correlated with the FWHM of the optical Balmer lines, though the Paschen lines have systematically lower FWHM values compared with the Balmer lines (though see F. Ricci et al. 2017b, who find no such offset). D. Kim et al. (2010) attribute this correlation to the Paschen lines also forming within the BLR but at a further distance from the black hole compared with the Balmer lines due to ionization stratification where the gas producing the Paschen lines is orbiting at a lower speed. Assuming the motion of the gas producing the Paschen lines is dominated by its orbital velocity around the SMBH, virial black hole mass formulas based on the FWHM of Paschen lines and either luminosity of these emission lines or NIR continuum luminosity can be used to estimate M_{BH} (D. Kim et al. 2010; H. Landt et al. 2011a, 2011b, 2013).

Here we test whether there is a correlation between $\log(L_{[\mathrm{O\ III}]}/L_{\mathrm{nH}\beta})$ and the FWHM of Paα and Paβ such that we may expect whether or not there would be agreement in the black hole masses derived using Equation (1) and the Paschen virial black hole mass equations. We plot these quantities in Figure 2 and find a significant correlation between $\log(L_{[\mathrm{O\ III}]}/L_{\mathrm{nH}\beta})$ and $\log(\mathrm{FWHM}_{\mathrm{Pa}\alpha})$ (Pearson correlation coefficient = 0.58, with p-value = 0.0297) though an insignificant correlation between $\log(L_{[\mathrm{O\ III}]}/L_{\mathrm{nH}\beta})$ and $\log(\mathrm{FWHM}_{\mathrm{Pa}\beta})$ (Pearson correlation coefficient = 0.508, p-value = 0.0918).

For comparison, we also include a line marking the expected relationship between $\log(L_{[\mathrm{O\ III}]}/L_{\mathrm{nH}\beta})$ and $\log(\mathrm{FWHM}_{\mathrm{Pa}\alpha})$ and

Table 4
Comparison of $\lambda L_{5100\ \text{Å}}$ Proxies and Black Hole Masses

x	y	Mean Offset[a] (dex)	Dispersion[a] (dex)	R[b]	p[b]	Slope[c]	Intercept[c]	σ_{residual}[d]	n[e]
$\lambda L_{5100\ \text{Å,nel}}$	$\lambda L_{5100\ \text{Å,X-ray}}$	−0.32	0.68	0.6565	1.6×10^{-13}	0.72 ± 0.08	-0.48 ± 0.08	0.65	99
$M_{\text{BH,Pa}\alpha}$	$M_{[\text{O III}]/\text{nH}\beta}$	0.39	0.44	0.7105	0.004	0.49 ± 0.14	4.42 ± 1.11	0.32	14
$M_{\text{BH,Pa}\beta}$	$M_{[\text{O III}]/\text{nH}\beta}$	0.48	0.51	0.6850	0.014	0.57 ± 0.19	3.71 ± 1.47	0.45	12
M_{BH,σ_*}	$M_{\text{BH,Pa}\alpha}$	0.08	0.33	0.8694	0.0002	0.93 ± 0.17	0.63 ± 1.30	0.36	12
M_{BH,σ_*}	$M_{\text{BH,Pa}\beta}$	−0.38	0.35	0.8719	0.0010	0.95 ± 0.19	0.02 ± 1.49	0.39	10
M_{BH,σ_*}	$M_{[\text{O III}]/\text{nH}\beta}$	−0.08	0.74	0.3327	3.0×10^{-5}	0.40 ± 0.09	4.78 ± 0.75	0.66	151

Notes.
[a] The mean offset and dispersion is calculated from $\log(y)$ to $\log(x)$. These results are equivalent to fitting a line between these parameters where the slope is fixed to unity and the offset represents the y-intercept.
[b] R is the Pearson correlation coefficient and p is the p-value used to measure the significance of a correlation. A p-value < 0.05 indicates a significant ($\geqslant 2\sigma$) correlation. Quoted results are from the PEARSONR function in SCIPY.
[c] Fitted slope and intercept from a linear fit to the quantities using LINEARLSQFITTER in astropy.
[d] Standard deviation in the fit residuals, calculated using $\sqrt{\sum_{i=1}^{n} \frac{(y_i - \hat{y})^2}{(n-2)}}$, where y_i is the measured value, $\hat{y}$ is the predicted value from the fitted relation, and n is the number of data points.
[e] Number of sources in sample.

$\log(\text{FWHM}_{\text{Pa}\beta})$ using Equation (1) from BM19 and the relationships found between the Hα FWHM and Paα and Paβ FWHM from D. Kim et al. (2010):

$$\log\left(\frac{\text{FWHM}_{\text{H}\alpha}}{1000\ \text{km s}^{-1}}\right) = (0.934 \pm 0.084) \times \log\left(\frac{\text{FWHM}_{\text{Pa}\alpha}}{1000\ \text{km s}^{-1}}\right) + (0.074 \pm 0.038), \quad (7)$$

$$\log\left(\frac{\text{FWHM}_{\text{H}\alpha}}{1000\ \text{km s}^{-1}}\right) = (0.821 \pm 0.075) \times \log\left(\frac{\text{FWHM}_{\text{Pa}\beta}}{1000\ \text{km s}^{-1}}\right) + (0.076 \pm 0.038). \quad (8)$$

Combining these equations with Equation (1) from BM19, we have:

$$\log\left(\frac{L_{[\text{O III}]}}{L_{\text{nH}\beta}}\right) = (0.54 \pm 0.08) \times \log\left(\frac{\text{FWHM}_{\text{Pa}\alpha}}{\text{km s}^{-1}}\right) - (1.22 \pm 0.73), \quad (9)$$

$$\log\left(\frac{L_{[\text{O III}]}}{L_{\text{nH}\beta}}\right) = (0.48 \pm 0.07) \times \log\left(\frac{\text{FWHM}_{\text{Pa}\beta}}{\text{km s}^{-1}}\right) - (1.02 \pm 0.60). \quad (10)$$

Though there is wide scatter in both relationships, it is striking that the measured $\log(L_{[\text{O III}]}/L_{\text{nH}\beta})$ values are systematically higher than the predicted trend line shown in Figure 2. Comparing these results with Figure 4 of BM19, which plots the relationship between $\log(L_{[\text{O III}]}/L_{\text{nH}\beta})$ and $\log(\text{FWHM}_{\text{bH}\alpha})$, we see that the measurements of $\log(L_{[\text{O III}]}/L_{\text{nH}\beta})$ from individual spectra are systematically higher than those derived from the stacked spectra and their derived trend line, similar to what we see in Figure 2. BM19 acknowledge that there is a weaker relationship between $\log(L_{[\text{O III}]}/L_{\text{nH}\beta})$ and $\log(\text{FWHM}_{\text{bH}\alpha})$ when considering line measurements from individual spectra compared with the median spectra from which they derived their Equation (1). They attribute this weaker correlation, and systematically higher $(L_{[\text{O III}]}/L_{\text{nH}\beta})$ ratio, to uncertainties in decomposing the nHβ line from the broad line, which underestimates the nHβ flux.

As our sample is not afflicted by similar uncertainties in the Hβ line decomposition, we conclude that the correlation between ionization field hardness and the FWHM of the broad Paschen lines is weaker than that reported for the broad Hα line. It could be that trends between NLR ionization hardness

Table 5
BASS Active Galactic Nucleus Black Hole Masses[a]

ID	$\log(M_{[\text{O III}]/\text{nH}\beta})$ $(M_\odot)$	$\log(M_{\text{BH,Pa}\alpha})$ $(M_\odot)$	$\log(M_{\text{BH,Pa}\beta})$ $(M_\odot)$	$\log(M_{\text{BH},\sigma_*})$ $(M_\odot)$
63	6.80	⋯	6.46	7.29
72	8.73	8.19	8.03	8.06
226	8.13	7.94	7.88	⋯
404	8.17	7.21	⋯	6.86
511	8.16	7.75	6.99	7.56
586	8.14	7.66	⋯	8.14
682	7.56	⋯	7.89	8.71
698	8.65	8.35	⋯	8.3
700	8.90	8.13	⋯	7.9
738	7.68	7.34	⋯	7.37
757	9.03	8.54	8.67	8.4
971	8.65	8.94	⋯	8.12
1027	7.96	⋯	7.46	7.85
1060	7.94	8.3	8.02	8.35
1090	8.00	8.22	8.04	⋯
1138	8.68	⋯	7.57	8.34
1157	7.58	6.41	6.2	6.3
1161	8.14	7.47	7.73	7.93

Note.
[a] $M_{[\text{O III}]/\text{nH}\beta}$, $M_{\text{BH,Pa}\alpha}$, and $M_{\text{BH,Pa}\beta}$ are calculated here using emission line fluxes from K. Oh et al. (2022), I. Lamperti et al. (2017), F. Ricci et al. (2022), and J. S. den Brok et al. (2022), and the intrinsic 2–10 keV X-ray fluxes from C. Ricci et al. (2017a). Black hole masses are calculated from the stellar velocity dispersions (M_{BH,σ_*}) reported in M. J. Koss et al. (2022c). We show here a subset of this table for illustrative purposes. The catalog is available in its entirety online.

(This table is available in its entirety in machine-readable form in the online article.)

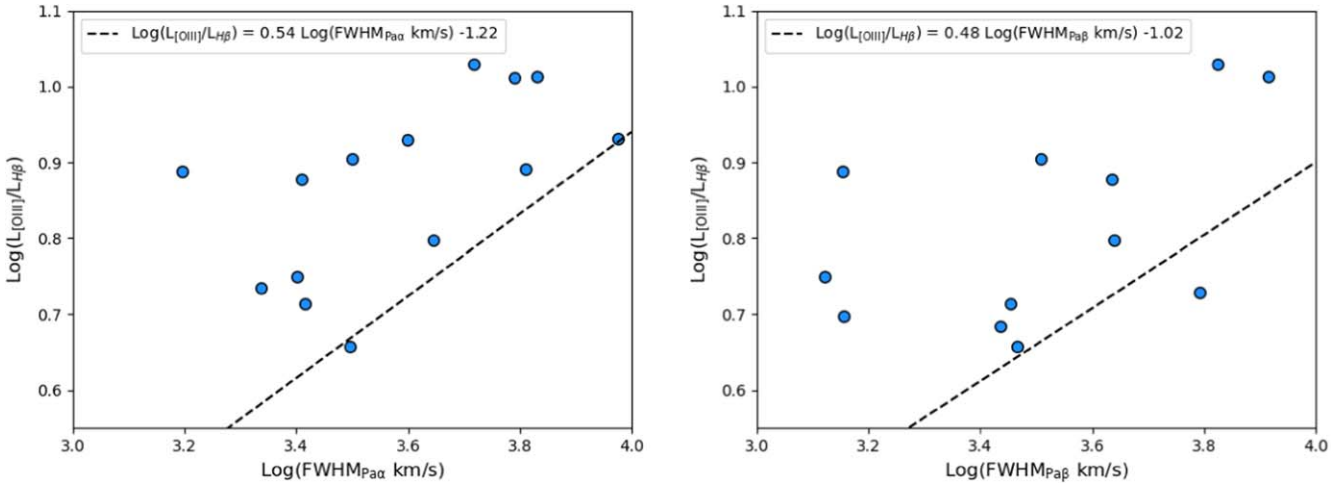

Figure 2. Comparison of NLR ionization field hardness ($\log(L_{[\mathrm{O\ III}]}/L_{\mathrm{nH}\beta})$) and BLR kinematics traced by the FWHM of the broad Paα (left) and Paβ (right) lines. We find a significant correlation between NLR ionization field hardness and $\mathrm{FWHM}_{\mathrm{Pa}\alpha}$ (p-value = 0.0297) but an insignificant correlation with $\mathrm{FWHM}_{\mathrm{Pa}\beta}$ (p-value = 0.0918). For reference, the expected relationship between $\log(L_{[\mathrm{O\ III}]}/L_{\mathrm{nH}\beta})$ and $\log(\mathrm{FWHM}_{\mathrm{Pa}\alpha})$ and $\log(\mathrm{FWHM}_{\mathrm{Pa}\beta})$, combining the results of D. Kim et al. (2010) and BM19 (Equations (9) and 10)), is shown by the dashed black line. The correlation between ionization field hardness and BLR kinematics is weaker than that reported in BM19. Either such trends are only prominent when considering aggregate AGN spectra (as in BM19) and not individual measurements, the coupling between the NLR ionization field and the more distant BLR in which the Paschen lines form is weaker, or extinction in the BLR that extinguishes broad Hα in these AGN also depresses the Paschen emission relative to the unobscured AGN studied in BM19. Error bars are not shown here since they are generally smaller than the size of the symbols.

and BLR kinematics are stronger when considering the AGN population in aggregate, as was done in BM19, rather than individually. Or there may be a physical driver: if the BLR is ionization stratified and the Paschen lines form further out from the center of the accretion disk than the Balmer lines, then perhaps there is a weaker coupling between the NLR ionization hardness and outer BLR compared with the inner BLR. Additionally, the AGN in this analysis are moderately obscured while BM19 analyzed Type 1, unobscured AGN; extinction toward the BLR may depress the broad Paschen lines causing the narrow [O III]/Hβ line ratio to appear relatively enhanced.

3.3. Comparing $L_{[O\ III]}/L_{nH\beta}$-derived M_{BH} with Paschen-derived M_{BH}

We use the following formulas from J. S. den Brok et al. (2022), originally published in D. Kim et al. (2010) but assuming a virial factor of $f = 1$, to calculate black hole masses from the NIR Paschen lines:

$$\log\left(\frac{M_{\mathrm{BH,Pa}\alpha}}{M_{\odot}}\right) = 7.16 + 0.43 \times \log\left(\frac{L_{\mathrm{Pa}\alpha}}{10^{42}\ \mathrm{erg\ s^{-1}}}\right) + 1.92 \times \log\left(\frac{\mathrm{FWHM}_{\mathrm{Pa}\alpha}}{10^{3}\ \mathrm{km\ s^{-1}}}\right), \quad (11)$$

$$\log\left(\frac{M_{\mathrm{BH,Pa}\beta}}{M_{\odot}}\right) = 7.20 + 0.45 \times \log\left(\frac{L_{\mathrm{Pa}\beta}}{10^{42}\ \mathrm{erg\ s^{-1}}}\right) + 1.69 \times \log\left(\frac{\mathrm{FWHM}_{\mathrm{Pa}\beta}}{10^{3}\ \mathrm{km\ s^{-1}}}\right). \quad (12)$$

In Table 5, we list the black hole masses calculated from these formulas for the AGN that have reliable fits to the broad Paα or Paβ lines.

In Figure 3, we compare $M_{\mathrm{BH,[O\ III]/nHn}\beta}$ with those calculated from the Paschen lines using the equations above, acknowledging that the marginal correlation found between $\log(L_{[\mathrm{O\ III}]}/L_{\mathrm{nH}\beta})$ and $\mathrm{FWHM}_{\mathrm{Pa}\beta}$ suggests that the relationship between the black hole masses calculated from these quantities may show poor agreement. Consistent with those expectations, we find a worse agreement between $M_{\mathrm{BH,[O\ III]/nH}\beta}$ and $M_{\mathrm{BH,Pa}\beta}$ ($p = 0.014$) than between $M_{\mathrm{BH,[O\ III]/nH}\beta}$ and $M_{\mathrm{BH,Pa}\alpha}$ ($p = 0.004$). $M_{\mathrm{BH,[O\ III]/nH}\beta}$ is systematically higher than the black hole masses derived from the Paschen lines, by an average factor of 0.39 $\pm$ 0.44 dex and 0.48 $\pm$ 0.51 dex for $M_{\mathrm{BH,Pa}\alpha}$ and $M_{\mathrm{BH,Pa}\beta}$, respectively. In both cases, we find a fitted slope that is shallower than unity. However, the residuals we find when fitting a linear relationship to the black hole mass proxies is consistent with the residuals when assuming a fixed slope of unity (see Table 4).

Since J. S. den Brok et al. (2022) do not report the quality of their spectral fits while the other two BASS NIR catalogs we queried did (I. Lamperti et al. 2017; F. Ricci et al. 2022), we investigate the impact that censoring these data have on our results. In Figure 3, we mark the AGN with J. S. den Brok et al. (2022) Paschen emission line measurements with dark green squares. When we remove these data points and repeat the analysis above, we find a better average agreement between $M_{\mathrm{BH,[O\ III]/nH}\beta}$ and $M_{\mathrm{BH,Pa}\alpha}$ (average offset of 0.30 $\pm$ 0.42 dex) and much closer agreement between $M_{\mathrm{BH,[O\ III]/nH}\beta}$ and $M_{\mathrm{BH,Pa}\beta}$ (average offset of 0.09 $\pm$ 0.26 dex), but this censoring only leaves us with six AGN in the Paβ sample.

Though the BASS AGN sample represents one of the most comprehensive AGN data sets, boasting rich optical, NIR, and X-ray spectroscopy (I. Lamperti et al. 2017; C. Ricci et al. 2017a; F. Ricci et al. 2017b; J. S. den Brok et al. 2022; M. J. Koss et al. 2022c; K. Oh et al. 2022), this analysis is still statistically limited with only 14 (12) AGN that have measured broad Paα (Paβ) emission. However, these results allow us to comment on trends and provide context for studies that use the BM19 method to estimate black hole mass (A. Ferré-Mateu et al. 2021; S.-C. Rey et al. 2021; G. Vietri et al. 2022; M. Siudek et al. 2023) and as an observational benchmark for theoretical simulations (F. Shankar et al. 2020; M. Volonteri et al. 2020; Y. Dubois et al. 2021; M. Habouzit et al. 2021; M. Trebitsch et al. 2021; A. Trinca et al. 2022; R. S. Beckmann et al. 2023; F. Sassano et al. 2023).

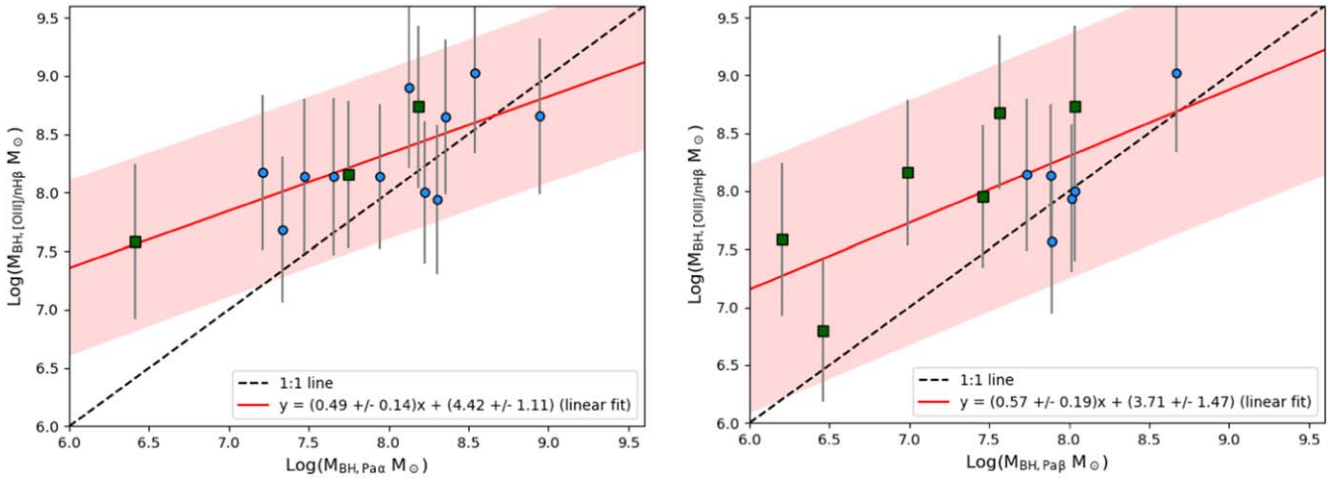

Figure 3. Comparison of black hole masses calculated using the $L_{[\mathrm{O\ III}]}/L_{\mathrm{nH}\beta}$ method in Equation (1) ($M_{\mathrm{BH,[O\ III]/nH}\beta}$) and those derived from the broad Paα line (left) and broad Paβ line (right). The dark green squares indicate AGN whose Paschen emission line parameters were derived from the J. S. den Brok et al. (2022) catalog where the quality of the spectral fit is not reported. $M_{\mathrm{BH,[O\ III]/nH}\beta}$ is systematically larger than masses derived via the broad Paschen lines by a factor of $\sim$2−3, though the scatter is slightly larger than these offsets (see Table 4). The agreement between the Paschen-derived black hole masses and those from the $L_{[\mathrm{O\ III}]}/L_{\mathrm{nH}\beta}$ method is better when censoring the J. S. den Brok et al. (2022) data (with mean offsets of 0.30 ± 0.42 dex and 0.09 ± 0.26 dex when comparing $M_{\mathrm{BH,[O\ III]/nHn\beta}}$ with $M_{\mathrm{BH,Pa}\alpha}$ and $M_{\mathrm{BH,Pa}\beta}$, respectively), but small number statistics preclude us from drawing conclusions from this censored data set. Error bars are derived by propagating the 0.68 dex uncertainty on $\lambda L_{5100\ \text{Å}}$ and the uncertainties on $\mathrm{FWHM_{bH}}\alpha$ (from the errors on the slope and normalization in Equation (2)) to the $M_{\mathrm{BH,[O\ III]/nH}\beta}$ equation (Equation (1)).

It is typical to find a factor of a few spread in black hole mass measurements using different methods. For instance, mass measurements using virial black hole mass formulas from the Balmer lines can be discrepant with direct mass measurements (i.e., measuring gas or stellar dynamics, or reverberation mapping) by a factor of 0.3–0.5 dex (e.g., B. M. Peterson 2014). At higher redshift, the uncertainties in black hole masses derived via reverberation mapping campaigns and single-epoch virial mass formulas are as high as 0.45 dex for Mg II and 0.58 for C IV. A similar comparison to what we have presented here is to compare black holes masses calculated from single-epoch virial mass formulas. Here too, comparisons between M_{BH} derived from C IV, Mg II, Hβ, and Hα show a spread of $\sim$0.12–0.40 dex (Y. Shen & X. Liu 2012; B. Trakhtenbrot & H. Netzer 2012).

By comparison, the dispersion in $\log(M_{\mathrm{BH,[O\ III]/nH}\beta}) - \log(M_{\mathrm{BH,Pa}\alpha})$ is on the high tail of the distribution found from intercomparisons of optical and ultraviolet broad-line virial mass measurements though similar to the dispersion found when comparing black holes masses calculated from reverberation mapping with those measured from single-epoch spectroscopy. However, the systematic offset between $M_{\mathrm{BH,[O\ III]/nH}\beta}$ and $M_{\mathrm{BH,Pa}\alpha}$ is higher than what is typically observed in these intercomparisons ($\sim$0.05–0.2 dex). The agreement of Paschen-derived black hole masses with those calculated from reverberation mapping or Balmer line virial mass formulas is also tighter ($\sim$0.2 dex; D. Kim et al. 2010) than we see in our comparison between $M_{\mathrm{BH,[O\ III]/nH}\beta}$ and the Paschen-derived black hole masses.

3.4. Masses Derived from the Stellar Velocity Dispersion

The well-known correlation between the central SMBH mass and the velocity dispersion of stars (σ_*) in the host galaxy (e.g., L. Ferrarese & D. Merritt 2000; K. Gebhardt et al. 2000) offers a method for calculating black hole masses from σ_* (M_{BH,σ_*}; L. Ferrarese et al. 2001). M. J. Koss et al. (2022c) measured the stellar velocity dispersions of 484 BASS AGN by using the penalized PPXF code (M. Cappellari & E. Emsellem 2004) to fit a model galaxy spectrum (using high-resolution galaxy templates) to the spectra of the BASS AGN host galaxies, observed mostly with the Very Large Telescope (VLT) X-shooter and Palomar/Double Spec. M. J. Koss et al. (2022c) used PPXF to calculate the velocity dispersions from the Ca II H and K $\lambda\lambda$3969, 3934, Mg I λ5175, and Ca II triplet $\lambda\lambda\lambda$8498, 8542, 8662 absorption lines (see M. J. Koss et al. 2022c, for full details). From the velocity dispersions, they calculated black hole masses using this relation from J. Kormendy & L. C. Ho (2013):

$$\log\left(\frac{M_{\mathrm{BH},\sigma_*}}{M_\odot}\right) = 4.38 \times \log\left(\frac{\sigma_*}{200\ \mathrm{km\ s^{-1}}}\right) + 8.49. \quad (13)$$

We report M_{BH,σ_*} for the BASS AGN used in this analysis in Table 5.

First, we compare the stellar velocity-dispersion-derived black hole masses with those calculated from the Paschen lines to test whether any systematic offsets are seen that are similar to what we observed in our $M_{\mathrm{BH,[O\ III]/nH}\beta}$ analysis above. As we show in Figure 4 and report in Table 4, a systematic offset is seen between M_{BH,σ_*} and the Paβ-derived black hole mass (−0.38 dex with a dispersion of 0.35 dex), though there is much better agreement with the Paα-derived black hole mass (0.08 dex with a dispersion of 0.33 dex). These results, when considered with the analysis above, indicate that the Paβ-derived black hole masses used in this analysis may be biased low.

We compare the $L_{[\mathrm{O\ III}]}/L_{\mathrm{nH}\beta}$-derived black hole masses with the stellar velocity-dispersion-derived black hole masses in Figure 5. There is a wide dispersion between values (0.74 dex), but these two methods of calculating black hole masses are in much better agreement (average $\log(M_{\mathrm{BH,[O\ III]/nH}\beta}) - (M_{\mathrm{BH},\sigma_*}) = -0.08$ dex) than when comparing $M_{\mathrm{BH,[O\ III]/nH}\beta}$ with the Paschen-derived black hole masses.

BM19 also compared $M_{\mathrm{BH,[O\ III]/nH}\beta}$ with the stellar velocity dispersion and stellar mass of the AGN host galaxies for the

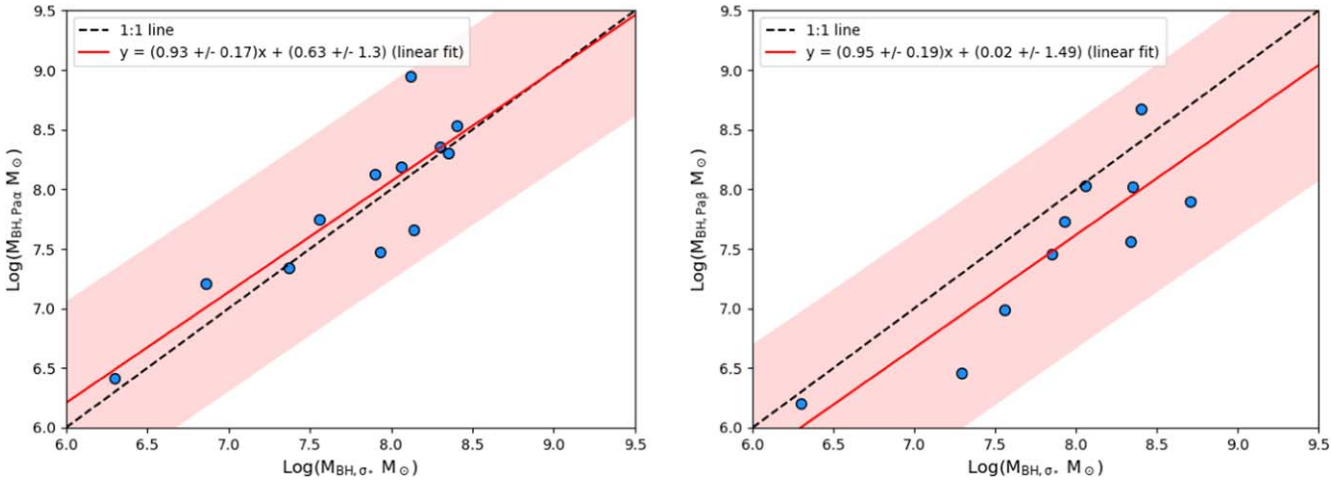

Figure 4. Comparison of black hole masses calculated from the host stellar velocity dispersion (M_{BH,σ_*}) and from the broad Paα line (left) and broad Paβ line (right). While there is a good agreement with $M_{\mathrm{BH,Pa}\alpha}$ (average offset of -0.08 dex with a standard deviation of 0.33 dex), M_{BH,σ_*} is systematically higher than $M_{\mathrm{BH,Pa}\beta}$ by a factor of 0.38 ± 0.35 dex, though the quantities are consistent with the one-to-one relation at the 95% prediction level. Line styles are the same as Figure 1.

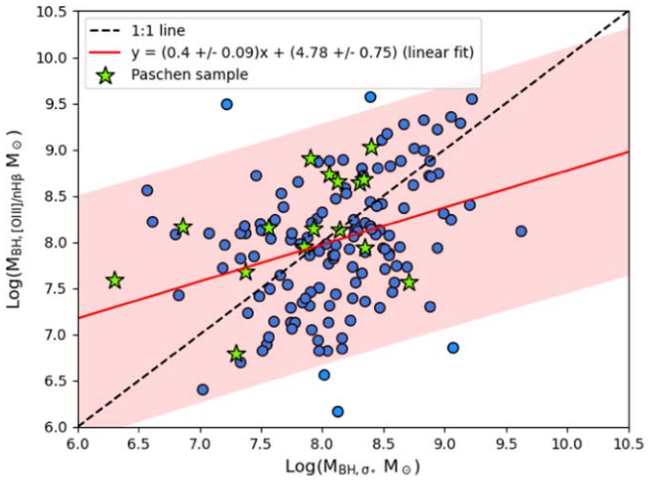

Figure 5. Comparison of $L_{[\mathrm{O\ III}]}/L_{\mathrm{nH}\beta}$-derived black hole masses ($M_{\mathrm{BH},[\mathrm{O\ III}]/\mathrm{nH}\beta}$) and those calculated from the host stellar velocity dispersion (M_{BH,σ_*}). For reference, the AGN we used to assess the agreement between $M_{\mathrm{BH},[\mathrm{O\ III}]/\mathrm{nH}\beta}$ and the Paschen-derived black hole masses are shown by the green stars. On average, the values are consistent to within 0.08 dex, albeit with a wide scatter (0.74 dex). Line styles are the same as Figure 1.

10,000 Type 2 SDSS AGN they analyzed. They performed a maximum likelihood estimation to quantify the relationship between $M_{\mathrm{BH},[\mathrm{O\ III}]/\mathrm{nH}\beta}$ and σ_*, finding a scatter of 0.45 dex (standard deviation). They thus conclude that their method provides black hole mass estimates as accurate as those derived from the $M_{\mathrm{BH}}-\sigma^*$ relation, though they stress that a direct test would come by comparing $M_{\mathrm{BH},[\mathrm{O\ III}]/\mathrm{nH}\beta}$ with those derived from the broad Paschen lines.

Finally we note that two of the BASS AGN we analyzed here have black hole masses measured via water megamaser disks (J. E. Greene et al. 2016): NGC 1194 and Circinus. We find a consistent M_{BH} value between the megamaser method and the BM19 method for NGC 1194 (7.85 dex compared with 7.95 dex, respectively), but a disagreement of almost 2 dex between these methods for Circinus (6.06 dex compared with 7.95 dex, respectively). The disagreement for Circinus could be due to its much closer proximity ($z = 0.0015$) compared with the typical SDSS AGN from which the BM19 value was derived ($0.01 < z < 0.3$): the optical spectra from Circinus were observed with the VLT using a $2''$ wide spectral slit (M. J. Koss et al. 2022a), so only the inner 60 pc of this galaxy was sampled, while the size scales probed by the SDSS AGN are 0.6–1.2 kpc. If the $L_{[\mathrm{O\ III}]}/L_{\mathrm{nH}\beta}$ ratio changes appreciably from circumnuclear scales (tens of parsecs) to extended scales (hundreds of parsecs), then the relationship calibrated using data extracted from a larger region may not be appropriate when applied to much smaller physical scales. For instance, SDSS MaNGA observations of nearby AGN demonstrate that $L_{[\mathrm{O\ III}]}/L_{\mathrm{nH}\beta}$ can sometimes be elevated closer to the black hole compared with extended scales (e.g., M. Albán & D. Wylezalek 2023) which would boost the M_{BH} value calculated from Equation (1) when measuring $L_{[\mathrm{O\ III}]}/L_{\mathrm{nH}\beta}$ from a compact region.

3.5. Properties of Obscured Active Galactic Nuclei in BASS

M. J. Koss et al. (2022c) reported the distribution of black hole masses (calculated from σ_*) and Eddington ratios ($L_{\mathrm{bol}}/L_{\mathrm{Edd}}$, where L_{bol} is the AGN bolometric luminosity and L_{Edd} is the Eddington luminosity, $L_{\mathrm{Edd}} = 1.26 \times 10^{38}\ M_{\mathrm{BH}}/M_{\odot}$) of obscured AGN (Type 1.9 and Type 2) from the BASS survey. Using the $M_{\mathrm{BH},[\mathrm{O\ III}]/\mathrm{nH}\beta}$ values we calculated, we compare the distribution of M_{BH} and Eddington ratios of this sample with the larger BASS sample from M. J. Koss et al. (2022c). To be consistent with the methodology of M. J. Koss et al. (2022c), we calculate L_{bol} from the intrinsic 14–150 keV luminosity reported in C. Ricci et al. (2017a) and use a bolometric correction factor of 8 (R. V. Vasudevan & A. C. Fabian 2009). Using the σ_* values reported in M. J. Koss et al. (2022c) and X-ray luminosities reported in C. Ricci et al. (2017a), we calculate M_{BH,σ_*} and the Eddington ratio for 323 obscured AGN from the BASS sample.

The distribution of M_{BH} and the Eddington ratio for both our $M_{\mathrm{BH},[\mathrm{O\ III}]/\mathrm{nH}\beta}$ sample and the BASS obscured AGN sample are shown in Figure 6. The distribution of black hole masses calculated via the BM19 method is similar to that of the larger BASS obscured AGN sample calculated via σ_* with a median $\log(M_{\mathrm{BH}}/M_{\odot})$ of 8.09 ± 0.73 (standard deviation) for our sample and 8.07 ± 0.59 for the BASS obscured AGN sample. There is a wider range in values of Eddington ratios for the BASS obscured AGN sample, indicating that the emission line ratio cuts we employ to create our $M_{\mathrm{BH},[\mathrm{O\ III}]/\mathrm{nH}\beta}$ sample

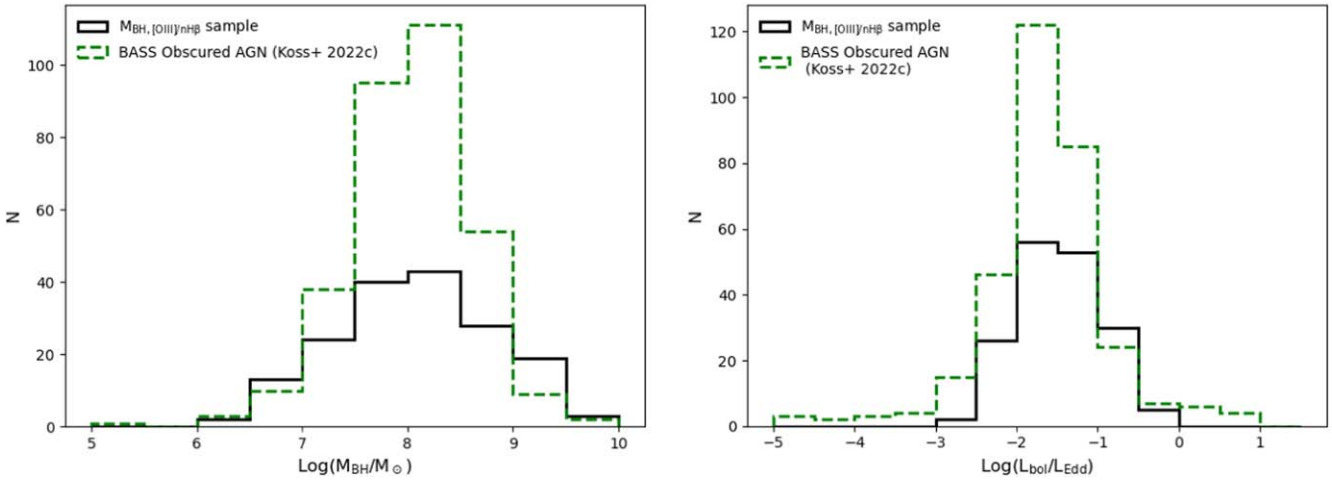

Figure 6. Comparison of $M_{\rm BH,[O\ III]/nH\beta}$ values from this study (black solid line) and $M_{\rm BH}$ derived from σ_* for a sample of 323 obscured BASS AGN (green dashed line; M. J. Koss et al. 2022a). The distributions are similar with median black hole mass values of $\log(M_{\rm BH}/L_\odot)$ of 8.09 ± 0.73 (standard deviation) and 8.07 ± 0.59 (standard deviation), respectively. Though there is large uncertainty in individual $M_{\rm BH,[O\ III]/nH\beta}$ measurements, the BM19 method provides a reasonable estimate of $M_{\rm BH}$ for a sample. Right: Eddington ratio ($L_{\rm bol}/L_{\rm Edd}$) distribution for our $M_{\rm BH,[O\ III]/nH\beta}$ sample and for the BASS obscured AGN sample. There is a much wider distribution of Eddington ratios for the BASS obscured AGN sample, indicating that the emission line ratio cuts we used remove AGN with extreme accretion rates, both at the low and high ends.

removes AGN accreting at low and high Eddington rates. The consistency between the distribution of $M_{\rm BH}$ between our sample and the BASS obscured AGN sample indicates that though there is large uncertainty in the black hole mass for any individual AGN, the BM19 method provides reasonable estimates of black hole masses for a population when other methods to measure $M_{\rm BH}$ are unavailable.

4. Conclusions

Using a sample of local AGN from the hard X-ray-selected BASS survey (M. Koss et al. 2017; M. J. Koss et al. 2022b) with intrinsic X-ray flux (C. Ricci et al. 2017a), optical spectroscopy (M. J. Koss et al. 2022b; K. Oh et al. 2022), and infrared spectroscopy (I. Lamperti et al. 2017; J. S. den Brok et al. 2022; F. Ricci et al. 2022) measurements, we tested the proposed method from BM19 to measure black hole masses in Type 2 (obscured) AGN that have ionization ratios between 0.55 dex $<$ $\log(L_{\rm [O\ III]}/L_{\rm nH\beta})$ $<$ 1.05 dex. This technique requires proxies for the FWHM of Hα and optical accretion disk luminosity ($\lambda L_{5100\ \text{Å}}$) in the black hole mass formula (Equation (1)) since these parameters are not visible in obscured AGN. BM19 demonstrated that the ionization field hardness in the extended NLR (parameterized by $L_{\rm [O\ III]}/L_{\rm nH\beta}$) correlates with the kinematics of gas in the BLR and can thus be used as a proxy of $\rm FWHM_{bH,\alpha}$ (Equation (2)).

Using a sample of 99 Type 2 AGN, we compared two methods for estimating $\lambda L_{5100\ \text{Å}}$, one based on the optical narrow emission lines (H. Netzer 2009; J. C. Runnoe et al. 2012) and the other based on the intrinsic 2–10 keV luminosity (R. Maiolino et al. 2007; E. Lusso et al. 2010). We find an average offset of 0.32 ± 0.68 dex between these luminosity proxies. This scatter introduces an uncertainty of a factor of ∼2 when using the BM19 relationship. About half the uncertainty in black hole masses is due to this scatter. The other major contributor to black hole mass uncertainty results from the errors in the slope and normalization in the relationship to derive $\rm FWHM_{bH\alpha}$ from the $L_{\rm [O\ III]}/L_{\rm nH\beta}$ ratio (Equation (2)).

Using Equations (1), (2), and (6), we calculated black hole masses ($M_{\rm BH,[O\ III]/nH\beta}$) that we compared with virial mass measurements derived from the broad NIR Paschen lines (D. Kim et al. 2010; J. S. den Brok et al. 2022). For the 14 (12) AGN that have reliable broad Paα (Paβ) emission line measurements (Figure 3), we found average offsets of 0.39 ± 0.44 dex (0.48 ± 0.51 dex). Though the offset is within the scatter, and the 95% confidence interval on the linear fit overlaps the one-to-one relation, the black hole masses derived from the BM19 technique from this limited sample appear to be systematically higher than those calculated from the broad Paschen lines. There is tentative evidence that the Paβ-derived black hole masses may be biased low since $M_{\rm BH,Pa\beta}$ is systematically lower than both $M_{\rm BH,[O\ III]/nH\beta}$ and black hole masses derived from the stellar velocity dispersion. More data are needed to test whether the apparent offset in $M_{\rm BH,[O\ III]/nH\beta}$ is due to a small sample size. The dispersion between $M_{\rm BH,[O\ III]/nH\beta}$ and $M_{\rm BH,Pa\alpha}$ aligns (albeit on the high end) with both the intrinsic scatter seen in broad-line single-epoch spectrum virial mass calibrations (e.g., M. Vestergaard & B. M. Peterson 2006) and intercomparison of black hole masses from the broad-line single-epoch formulas (e.g., Y. Shen & X. Liu 2012; B. Trakhtenbrot & H. Netzer 2012).

When comparing $M_{\rm BH,[O\ III]/nH\beta}$ with black hole masses derived from the stellar velocity dispersion (J. Kormendy & L. C. Ho 2013; M. J. Koss et al. 2022c) for a sample of 151 AGN, there is better overall agreement (mean offset of 0.08 dex) though with much wider scatter (0.74 dex). This scatter is a factor of about 2–3 higher than the observed scatter in $M_{\rm BH}$–σ_* relationships (e.g., C. Marsden et al. 2020) and larger than the typical uncertainty of 0.5 dex ascribed to the BM19 method based on their quoted scatter in $M_{\rm BH,[O\ III]/nH\beta}$–$\sigma_*$.

We compare the black hole mass and Eddington ratio distribution for our $M_{\rm BH,[O\ III]/nH\beta}$ sample and a larger sample of obscured AGN from BASS, where $M_{\rm BH}$ was calculated from σ_*. The distributions are similar with nearly identical median $M_{\rm BH}$ values. This result indicates that the BM19 method gives a reasonable estimate of $M_{\rm BH}$ on the population level even if individual measurements have large uncertainties.

A number of theoretical studies have compared $M_{\rm BH}$ to host galaxy properties to glean insight into black hole and galaxy coevolution, and compared these predictions with

observational results that include $M_{\rm BH,[O\,III]/nH\beta}$ values from the sample of 10,000 SDSS Type 2 AGN reported in BM19 (F. Shankar et al. 2020; M. Volonteri et al. 2020; Y. Dubois et al. 2021; M. Habouzit et al. 2021; M. Trebitsch et al. 2021; A. Trinca et al. 2022; R. S. Beckmann et al. 2023; F. Sassano et al. 2023). A handful of other papers use the methodology described in BM19 to estimate black hole masses for Type 2 AGN (A. Ferré-Mateu et al. 2021; S.-C. Rey et al. 2021; G. Vietri et al. 2022; M. Siudek et al. 2023). By testing this indirect method with a more direct measurement of black hole mass from the NIR Paschen lines, we find that the scatter is on the high end of that observed when comparing often-used single-epoch spectroscopy broad-line virial mass formulas. Our results also suggest that $M_{\rm BH,[O\,III]/nH\beta}$ may be biased high compared with $M_{\rm BH}$ from the broad Paschen lines, though the offset is within the scatter and more data would be needed to confirm this tentative result. We conclude that Equations (2) and (6) (or Equations (3), (4), and (5), if the intrinsic 2–10 X-ray luminosity is unknown) can be used to estimate the black hole mass in obscured AGN when no other methods are feasible, though with the caveat that the uncertainty can be as high as 0.5–0.74 dex and the results may be biased high by a factor of $\sim$2−3.

We also caution that the correlation between $L_{\rm [O\,III]}/L_{\rm nH\beta}$ and $\rm FWHM_{bH,\alpha}$, which is the foundation for this BM19 $M_{\rm BH}$ estimate, has only been demonstrated for a limited parameter space: AGN with ionization ratios between 0.55 dex $<\log(L_{\rm [O\,III]}/L_{\rm nH\beta})<1.05$ dex that are not hosted in low-metallicity galaxies (see, e.g., M. Hirschmann et al. 2019; O. L. Dors et al. 2024), and are below a redshift of $z<1$ (i.e., the $L_{\rm [O\,III]}/L_{\rm nH\beta}$ ratio for star-forming galaxies increases with redshift, where local relations no longer hold starting at $z\sim1$; L. J. Kewley et al. 2013). This technique can be useful for providing black hole mass estimates for AGN detected in X-ray surveys and for obscured AGN discovered in spectroscopic surveys that have measurements of [O III], nHβ, and nHα within this parameter space. A similar investigation into the correlation between $L_{\rm [O\,III]}/L_{\rm nH\beta}$ and $\rm FWHM_{bH,\alpha}$ can be done in the future for AGN at higher redshift to identify whether such a trend as that reported in BM19 for lower-redshift AGN is present, and, if so, what range of $L_{\rm [O\,III]}/L_{\rm nH\beta}$ would be appropriate as a proxy of BLR kinematics for estimating black hole masses in high-redshift obscured AGN.

Acknowledgments

We thank the referees for insightful feedback that improved the quality of this manuscript. B.T. acknowledges support from the European Research Council (ERC) under the European Union's Horizon 2020 Research and Innovation program (grant agreement No. 950533) and from the Israel Science Foundation (grant No. 1849/19).

Software: astropy (Astropy Collaboration et al. 2013, 2018, 2022).

Appendix

We provide a derivation for Equation (6) in the main text, which we use to estimate $\lambda L_{5100\ \text{Å}}$ from the intrinsic 2–10 keV X-ray luminosity ($L_{2-10\ \rm keV}$). We begin with Equation (6) of E. Lusso et al. (2010), which relates the monochromatic X-ray luminosity at 2 keV ($L_{2\ \rm keV}$) to the monochromatic ultraviolet luminosity at 2500 Å ($L_{2500\ \text{Å}}$):

$$\log\left(\frac{L_{2\,\rm keV}}{\rm erg\ s^{-1}\,Hz^{-1}}\right)=0.760\times\log\left(\frac{L_{2500}}{\rm erg\ s^{-1}\,Hz^{-1}}\right)+3.508. \quad \text{(A1)}$$

This relation was calibrated using an X-ray selected sample of Type 1 AGN from the XMM-COSMOS survey (G. Hasinger et al. 2007; N. Cappelluti et al. 2009).

To calculate the monochromatic luminosity at 5100 Å, we use the ultraviolet–optical spectral slope calculated from the mean spectrum of Type 1 AGN in SDSS that is reported in D. E. Vanden Berk et al. (2001), $\alpha_\nu=-0.44$, where $f_\nu\propto\lambda^{-(\alpha_\nu+2)}$:

$$\frac{L_{2500}}{L_{5100}}=\left(\frac{2500}{5100}\right)^{-1(\alpha_\nu+2)}=\left(\frac{2500}{5100}\right)^{-1.56}=3.041. \quad \text{(A2)}$$

Substituting this relationship into the E. Lusso et al. (2010) relation gives:

$$\log\left(\frac{L_{2\,\rm keV}}{\rm erg\ s^{-1}\,Hz^{-1}}\right)=0.760\times\log\left(\frac{L_{5100}}{\rm erg\ s^{-1}\,Hz^{-1}}\right)+3.875. \quad \text{(A3)}$$

We then convert from monochromatic luminosity to $\lambda L_{5100\ \text{Å}}$ (in units of erg s^{-1}) using:

$$\left(\frac{\lambda L_{5100}}{\rm erg\ s^{-1}}\right)=\left(\frac{L_{5100}}{\rm erg\ s^{-1}\,Hz^{-1}}\right)\times\nu_{5100}$$
$$=\left(\frac{L_{5100}}{\rm erg\ s^{-1}\,Hz^{-1}}\right)\times5.878\times10^{14}\ \rm Hz. \quad \text{(A4)}$$

We convert the monochromatic 2 keV luminosity from units of erg s^{-1} Hz^{-1} to units of erg s^{-1} keV^{-1} using:

$$\left(\frac{L_{2\,\rm keV}}{\rm erg\ s^{-1}\,keV^{-1}}\right)=\left(\frac{L_{2\,\rm keV}}{\rm erg\ s^{-1}\,Hz^{-1}}\right)\times2.418\times10^{17}\frac{\rm Hz}{\rm keV}. \quad \text{(A5)}$$

To convert from monochromatic 2 keV luminosity to integrated 2–10 keV luminosity, we assume a standard X-ray spectral model for AGN where the X-ray spectral slope (Γ) is 1.8, which is the median Γ for Swift-BAT AGN (C. Ricci et al. 2017a). Using PIMMS,[9] we find:

$$L_{2-10\,\rm keV}=3.80\times L_{2\,\rm keV}. \quad \text{(A6)}$$

Substituting Equations (A4), (A5), and (A6) into Equation (A3), we derive:

$$\log\left(\frac{\lambda L_{5100}}{\rm erg\ s^{-1}}\right)=1.316\times\log\left(\frac{L_{2-10\,\rm keV}}{\rm erg\ s^{-1}}\right)-13.966. \quad \text{(A7)}$$

Finally, recasting this relation using normalized luminosities, we have:

$$\log\left(\frac{\lambda L_{5100}}{10^{44}\ \rm erg\ s^{-1}}\right)=1.316\times\log\left(\frac{L_{2-10\,\rm keV}}{10^{43}\ \rm erg\ s^{-1}}\right)-1.378. \quad \text{(A8)}$$

We note that the estimate of $\lambda L_{5100\ \text{Å}}$ that is derived from the intrinsic X-ray luminosity has a weak dependence on the assumed spectral slope of the X-ray power-law emission. Within the range of typical AGN Γ values of 1.7 (e.g., R. Maiolino et al. 2007) and 2.0 (e.g., V. Mainieri et al. 2007), which also represent the range of the median fitted spectral

[9] https://cxc.harvard.edu/toolkit/pimms.jsp

slope for different subsets of BAT AGN separated by column density (C. Ricci et al. 2017a) and AGN detected in other multiwavelength surveys like XMM-XXL (Z. Liu et al. 2016), Chandra Deep Field South (T. Liu et al. 2017), and Stripe 82X (A. Peca et al. 2023), the normalization in Equation (A8) ranges from -1.426 ($\Gamma = 1.7$) to -1.283 ($\Gamma = 2.0$). Consequently, $\log(\lambda L_{5100\ \text{Å}})$ can vary by a factor of 0.14 dex, which affects the estimated black hole mass by about 20% (0.08 dex).

ORCID iDs

Stephanie LaMassa https://orcid.org/0000-0002-5907-3330
C. Megan Urry https://orcid.org/0000-0002-0745-9792
Benny Trakhtenbrot https://orcid.org/0000-0002-3683-7297
Connor Auge https://orcid.org/0000-0002-5504-8752
Michael J. Koss https://orcid.org/0000-0002-7998-9581
Alessandro Peca https://orcid.org/0000-0003-2196-3298
Dave Sanders https://orcid.org/0000-0002-1233-9998
Tracey Jane Turner https://orcid.org/0000-0003-2971-1722

References

Abazajian, K. N., Adelman-McCarthy, J. K., Agüeros, M. A., et al. 2009, ApJS, 182, 543
Albán, M., & Wylezalek, D. 2023, A&A, 674, A85
Astropy Collaboration, Price-Whelan, A. M., Lim, P. L., et al. 2022, ApJ, 935, 167
Astropy Collaboration, Price-Whelan, A. M., Sipöcz, B. M., et al. 2018, AJ, 156, 123
Astropy Collaboration, Robitaille, T. P., Tollerud, E. J., et al. 2013, A&A, 558, A33
Baldwin, J. A., Phillips, M. M., & Terlevich, R. 1981, PASP, 93, 5
Baron, D., & Ménard, B. 2019, MNRAS, 487, 3404
Barthelmy, S. D., Barbier, L. M., Cummings, J. R., et al. 2005, SSRv, 120, 143
Bassani, L., Dadina, M., Maiolino, R., et al. 1999, ApJS, 121, 473
Beckmann, R. S., Dubois, Y., Volonteri, M., et al. 2023, MNRAS, 523, 5610
Bentz, M. C., Denney, K. D., Grier, C. J., et al. 2013, ApJ, 767, 149
Bentz, M. C., Peterson, B. M., Netzer, H., et al. 2009, ApJ, 697, 160
Bentz, M. C., Peterson, B. M., Pogge, R. W., et al. 2006, ApJ, 644, 133
Cappellari, M., & Emsellem, E. 2004, PASP, 116, 138
Cappelluti, N., Brusa, M., Hasinger, G., et al. 2009, A&A, 497, 635
Cardelli, J. A., Clayton, G. C., & Mathis, J. S. 1989, ApJ, 345, 245
Charlot, S., & Fall, S. M. 2000, ApJ, 539, 718
den Brok, J. S., Koss, M. J., Trakhtenbrot, B., et al. 2022, ApJS, 261, 7
Dors, O. L., Cardaci, M. V., Hagele, G. F., et al. 2024, MNRAS, 527, 8193
Dubois, Y., Beckmann, R., Bournaud, F., et al. 2021, A&A, 651, A109
Ferrarese, L., & Merritt, D. 2000, ApJL, 539, L9
Ferrarese, L., Pogge, R. W., Peterson, B. M., et al. 2001, ApJL, 555, L79
Ferré-Mateu, A., Mezcua, M., & Barrows, R. S. 2021, MNRAS, 506, 4702
Gebhardt, K., Bender, R., Bower, G., et al. 2000, ApJL, 539, L13
Gehrels, N., Chincarini, G., Giommi, P., et al. 2004, ApJ, 611, 1005
Genzel, R., Eisenhauer, F., & Gillessen, S. 2010, RvMP, 82, 3121
Genzel, R., Pichon, C., Eckart, A., et al. 2000, MNRAS, 317, 348
Ghez, A. M., Klein, B. L., Morris, M., et al. 1998, ApJ, 509, 678
Ghez, A. M., Salim, S., Weinberg, N. N., et al. 2008, ApJ, 689, 1044
Gliozzi, M., Williams, J. K., Akylas, A., et al. 2024, MNRAS, 528, 3147
Greene, J. E., & Ho, L. C. 2005, ApJ, 630, 122
Greene, J. E., Peng, C. Y., & Ludwig, R. R. 2010, ApJ, 709, 937
Greene, J. E., Seth, A., Kim, M., et al. 2016, ApJL, 826, L32
Grier, C. J., Shen, Y., Horne, K., et al. 2019, ApJ, 887, 38
Grier, C. J., Trump, J. R., Shen, Y., et al. 2017, ApJ, 851, 21
Gültekin, K., Richstone, D. O., Gebhardt, K., et al. 2009, ApJ, 698, 198
Habouzit, M., Li, Y., Somerville, R. S., et al. 2021, MNRAS, 503, 1940
Hasinger, G., Cappelluti, N., Brunner, H., et al. 2007, ApJS, 172, 29
Hickox, R. C., & Alexander, D. M. 2018, ARA&A, 56, 625
Hirschmann, M., Charlot, S., Feltre, A., et al. 2019, MNRAS, 487, 333
Homayouni, Y., Trump, J. R., Grier, C. J., et al. 2020, ApJ, 901, 55
Kaspi, S., Maoz, D., Netzer, H., et al. 2005, ApJ, 629, 61
Kewley, L. J., Dopita, M. A., Sutherland, R. S., et al. 2001, ApJ, 556, 121
Kewley, L. J., Maier, C., Yabe, K., et al. 2013, ApJL, 774, L10
Kim, D., Im, M., & Kim, M. 2010, ApJ, 724, 386
Kormendy, J., & Ho, L. C. 2013, ARA&A, 51, 511
Kormendy, J., & Richstone, D. 1995, ARA&A, 33, 581
Koss, M., Trakhtenbrot, B., Ricci, C., et al. 2017, ApJ, 850, 74
Koss, M. J., Ricci, C., Trakhtenbrot, B., et al. 2022a, ApJS, 261, 2
Koss, M. J., Trakhtenbrot, B., Ricci, C., et al. 2022b, ApJS, 261, 1
Koss, M. J., Trakhtenbrot, B., Ricci, C., et al. 2022c, ApJS, 261, 6
LaMassa, S. M., Heckman, T. M., Ptak, A., et al. 2009, ApJ, 705, 568
LaMassa, S. M., Heckman, T. M., Ptak, A., et al. 2010, ApJ, 720, 786
LaMassa, S. M., Yaqoob, T., Tzanavaris, P., et al. 2023, ApJ, 944, 152
Lamperti, I., Koss, M., Trakhtenbrot, B., et al. 2017, MNRAS, 467, 540
Landt, H., Bentz, M. C., Peterson, B. M., et al. 2011a, MNRAS, 413, L106
Landt, H., Elvis, M., Ward, M. J., et al. 2011b, MNRAS, 414, 218
Landt, H., Ward, M. J., Peterson, B. M., et al. 2013, MNRAS, 432, 113
Liu, T., Tozzi, P., Wang, J.-X., et al. 2017, ApJS, 232, 8
Liu, Z., Merloni, A., Georgakakis, A., et al. 2016, MNRAS, 459, 1602
Lusso, E., Comastri, A., Vignali, C., et al. 2010, A&A, 512, A34
Mainieri, V., Hasinger, G., Cappelluti, N., et al. 2007, ApJS, 172, 368
Magorrian, J., Tremaine, S., Richstone, D., et al. 1998, AJ, 115, 2285
Maiolino, R., Shemmer, O., Imanishi, M., et al. 2007, A&A, 468, 979
Marsden, C., Shankar, F., Ginolfi, M., et al. 2020, FrP, 8, 61
Mejía-Restrepo, J. E., Trakhtenbrot, B., Koss, M. J., et al. 2022, ApJS, 261, 5
Misner, C. W., Thorne, K. S., & Wheeler, J. A. 1973, in Gravitation, ed. C. W. Misner, K. S. Thorne, & J. A. Wheeler (San Francisco, CA: Freeman),
Moran, J. M., Greenhill, L. J., & Herrnstein, J. R. 1999, JApA, 20, 165
Netzer, H. 2009, MNRAS, 399, 1907
Oh, K., Koss, M. J., Ueda, Y., et al. 2022, ApJS, 261, 4
Osterbrock, D. E. 1993, ApJ, 404, 551
Osterbrock, D. E., & Ferland, G. J. 2006, in Astrophysics of Gaseous Nebulae and Active Galactic Nuclei, ed. D. E. Osterbrock & G. J. Ferland (2; Sausalito, CA: Univ. Science Books),
Peca, A., Cappelluti, N., Urry, C. M., et al. 2023, ApJ, 943, 162
Peterson, B. M. 2014, SSRv, 183, 253
Planck Collaboration, Ade, P. A. R., Aghanim, N., et al. 2016, A&A, 594, A13
Ramos Almeida, C., & Ricci, C. 2017, NatAs, 1, 679
Reines, A. E., & Volonteri, M. 2015, ApJ, 813, 82
Rey, S.-C., Oh, K., & Kim, S. 2021, ApJL, 917, L9
Ricci, C., Trakhtenbrot, B., Koss, M. J., et al. 2017a, ApJS, 233, 17
Ricci, F., La Franca, F., & Marconi, A. 2017c, MNRAS, 471, L41
Ricci, F., La Franca, F., Onori, F., et al. 2017b, A&A, 598, A51
Ricci, F., Treister, E., Bauer, F. E., et al. 2022, ApJS, 261, 8
Runnoe, J. C., Brotherton, M. S., & Shang, Z. 2012, MNRAS, 422, 478
Sassano, F., Capelo, P. R., Mayer, L., et al. 2023, MNRAS, 519, 1837
Shankar, F., Allevato, V., Bernardi, M., et al. 2020, NatAs, 4, 282
Shen, Y., & Liu, X. 2012, ApJ, 753, 125
Shen, Y., Brandt, W. N., Dawson, K. S., et al. 2015, ApJS, 216, 4
Shen, Y., Grier, C. J., Horne, K., et al. 2024, ApJS, 272, 26
Shen, Y., Hall, P. B., Horne, K., et al. 2019, ApJS, 241, 34
Shen, Y., Richards, G. T., Strauss, M. A., et al. 2011, ApJS, 194, 45
Siudek, M., Mezcua, M., & Krywult, J. 2023, MNRAS, 518, 724
Tananbaum, H., Avni, Y., Branduardi, G., et al. 1979, ApJL, 234, L9
Trakhtenbrot, B., & Netzer, H. 2012, MNRAS, 427, 3081
Trebitsch, M., Dubois, Y., Volonteri, M., et al. 2021, A&A, 653, A154
Trinca, A., Schneider, R., Valiante, R., et al. 2022, MNRAS, 511, 616
Vanden Berk, D. E., Richards, G. T., Bauer, A., et al. 2001, AJ, 122, 549
Vasudevan, R. V., & Fabian, A. C. 2009, MNRAS, 392, 1124
Vestergaard, M., & Peterson, B. M. 2006, ApJ, 641, 689
Vietri, G., Garilli, B., Polletta, M., et al. 2022, A&A, 659, A129
Volonteri, M., Pfister, H., Beckmann, R. S., et al. 2020, MNRAS, 498, 2219
Woo, J.-H., Yoon, Y., Park, S., et al. 2015, ApJ, 801, 38
York, D. G., Adelman, J., Anderson, J. E., et al. 2000, AJ, 120, 1579
Zhu, G., Zaw, I., Blanton, M. R., et al. 2011, ApJ, 742, 73